Pergamon

Journal of Structural Geology, Vol. 17, No. 8, pp. 1095 to 1109, 1995

0191-8141/95 $9.50+0.00

0191-8141(95)00007-0

Quartz deformation in a very fine grained quartzo-feldspathic mylonite: a lack of evidence for dominant grain boundary sliding deformation

TIMON F. FLIERVOET and STANLEY H. WHITE

Faculty of Earth Sciences, Department of Geology, Utrecht University, P.O. Box 80.021, Budapestlaan 4, 3508 TA Utrecht, The Netherlands

(*Received* 7 *April* 1994; *accepted in revised form* 21 *December* 1994)

Abstract—Microstructural and microtextural investigations by transmission electron microscopy (TEM) have been performed on very fine grained quartzo-feldspathic mylonites from the Red Bank Deformed Zone, Central Australia. The study of the quartz reveals a mean grain size (2.3 ± 0.8 μm) and microstructural features indicative of dislocation creep processes within the very fine grained quartz. Analysis of local crystallographic preferred orientation (CPO) by TEM, showed a strong CPO for both the *c*- and *a*-axes. The crystallographic relationships between adjacent grains and subgrains are consistent with dominant $\langle c + a \rangle$ and $\langle a \rangle$ slip. Microstructural and microtextural studies also show that the recrystallization mechanism included local grain boundary migration and the formation of high angle grain boundaries from low angle (sub)grain boundaries by progressive misorientation. We found no abnormal grain rotations as would be expected to result from grain boundary sliding processes. This suggests that grain boundary sliding was not significant and the dominant deformation mechanism was dislocation creep.

INTRODUCTION

Major shear zones play a fundamental role in the deformation and dynamics of the earth's continental lithosphere. Many have exhibited multiple reactivations since their initiation and have been foci for much continental tectonism (Obee & White 1986, White *et al.* 1986). Such zones tend to traverse the entire continental crust, and probably extend deep into the upper mantle (e.g. McGeary & Warner 1985, Choukroune & ECORS-team 1989, Golby *et al.* 1989).

The reason that these zones are fundamental planes of weakness in the crust or upper mantle lies in the rocks (mylonites) that develop within them. It is commonly observed that deformation (strain) is partitioned into the finest grained parts of these zones (e.g. White 1976, 1979b,c, Watts & Williams 1979, White *et al.* 1980). Consequently the rheology of, and deformation within, these fine grained parts are of major significance in controlling both reactivation and the role that these major shears have in crustal and upper mantle dynamics.

In many rocks deforming under mid- to upper-crustal conditions, quartz forms the stress supporting framework (Vernon & Flood 1988). Under these conditions, the deformation leads to the familiar mesoscopic augen-gneiss structure formed by elongate quartz bands anastomosing around relatively undeformed or slightly deformed feldspar augen (Behrmann & Mainprice 1987). The plastic flow strength of the crust under these conditions is generally set by wet quartzite (e.g. White *et al.* 1986, Carter & Tsenn 1987, Ord & Hobbs 1989).

The deformation mechanisms of quartzose and quartz framework rocks have been studied in detail in both experimental (e.g. Tullis *et al.* 1973, Jaoul *et al.* 1984, Hirth & Tullis 1992) and natural creep (e.g. White 1973, 1976, Mitra 1976, Law *et al.* 1984, Behrmann 1985, Knipe & Law 1987, Lloyd *et al.* 1992). Intracrystalline plasticity by dislocation processes has been identified as an important deformation mechanism and there is evidence in the literature (White 1973, 1976, 1977, Bossière & Vauchez 1978, Berthé *et al.* 1979, Watts & Williams 1979, Simpson 1985) that it is one of the main factors controlling the deformation of quartzo-feldspathic granitoid rocks. It has been shown (e.g. White 1976, Etheridge & Wilkie 1979, Behrmann 1985, Lloyd *et al.* 1992) that with a decrease in grain size, the deformation mechanism in some cases changes from grain size insensitive to grain size sensitive flow with a major contribution of grain boundary sliding, a type of behaviour sometimes tentatively called superplasticity.

Behrmann (1985) inferred that this change occurred, in quartzite, at a grain size of 10 μm at temperatures around 250–400°C, from a switch in the relation between dislocation density and grain size from proportional to inverse. Other microstructural criteria often used to infer grain boundary sliding include (i) a diamond or blocky grain shape (White 1977, Drury & Humphreys 1988), (ii) a continuous alignment of grain boundaries over several grain diameters (White 1977, Stünitz & Fitz Gerald 1993), (iii) high dislocation densities at triple junctions, (iv) a grain size comparable to or smaller than the equilibrium subgrain size (White 1977, 1979b, Gapais & White 1982), (v) an inverse relation between finite strain and grain size (Evans *et al.* 1980), (vi) grain boundary voids at triple junctions (White 1977, Behrmann 1985), and (vii) a grain size generally less than 10 μm (Boullier & Gueguen 1975, White 1977, Behrmann 1985). In addition, any crystallographic preferred orien-

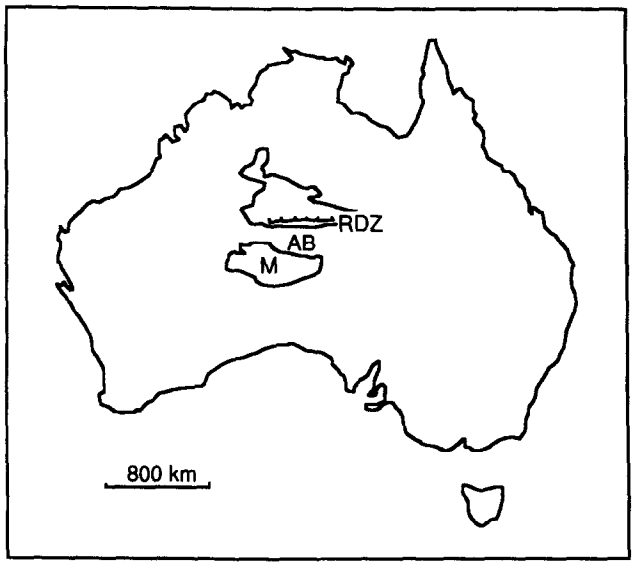

Fig. 1. Location map of the Redbank Deformed Zone (latitude 23°40′; longitude 129° to 134°). AB, Arunta Block; M, Musgrave Block; RDZ, Redbank Deformed Zone (after Obee & White 1985, 1986).

tation (CPO) generated should be weak (Padmanabhan & Davies 1980, pp. 111–117, Rutter *et al.* 1994) and due to grain rotations and neighbour switching events which accompany grain boundary sliding (Beeré 1978), there should be no crystallographic relation between adjacent grains. However, the microtextural evidence is difficult to obtain, especially in multiphase rocks, and there is uncertainty about the role of grain boundary sliding deformation in fine grained rocks.

In this paper we present a microstructural and microtextural study of quartz bands in a very fine grained (less than 10 μm) quartzo-feldspathic mylonite deformed at upper greenschist facies conditions, using both optical and electron optical techniques. The results are subsequently discussed in terms of dominant deformation mechanisms.

GEOLOGICAL SETTING AND SAMPLE LOCATION

The samples are from mylonites from the Redbank Deformed Zone (near Alice Springs, Central Australia, Fig. 1), which is a major shear-boundary separating a region of granulite facies rocks in the north from predominantly amphibolite facies rocks in the south (Shaw & Black 1991). The Redbank Deformed Zone is a major Proterozoic fault zone, with a complex history of multiple reactivation and when active formed part of a major thrust system in the Paleozoic (Shaw & Black 1991). Seismic reflection profiles show that the fault zone traverses the entire continental crust and extends into the upper mantle (Goleby *et al.* 1989). It is a complex zone of intense deformation, up to 8 km across, containing several narrow mylonite zones (typically a few centimeters to a few meters wide) formed at amphibolite to greenschist facies conditions (Obee & White 1985, Shaw & Black 1991). The mylonites are marked by a moderate to steep N-dipping mylonitic foliation with a down dip stretching lineation and a reverse movement sense.

The country rock, in which the mylonites have developed, includes migmatite, banded gneiss and slightly foliated granitic gneiss with large feldspar augen (Obee & White 1985, Shaw & Black 1991). With increasing strain, the matrix grain size decreases, the feldspar clasts decrease in size and form augen which commonly develop tails parallel to the mineral lineation (Fig. 2a). In the finest grained parts of the shear zones, most of these feldspar clasts are eventually assimilated into the matrix, leaving only a few small augen in the fine grained matrix (Fig. 2a). These rocks then have a black or very dark grey colour in hand specimen. The sample studied is from one of these shear zones: a narrow, dark mylonitic zone located in the southeastern part of the New Well area (grid reference: 7389500 N and 356600 E), an area previously studied by Obee & White (1985, 1986).

EXPERIMENTAL TECHNIQUES

Detailed optical studies were first undertaken on thin sections from fine and coarse grained bands within the mylonite and *c*-axis orientations were measured, where grain size permitted, by traditional universal stage techniques. Following these studies, electron-transparent foils (thickness <1 μm) of selected areas from the thin sections from the fine grained bands were prepared by ion-beam thinning. After thinning, the specimens were coated with a thin carbon layer to eliminate sample charging during observation. Transmission electron microscopy (TEM) analyses were carried out on a Philips CM20 operating at 200 kV. The TEM observations were made in standard bright-field (BF) and diffraction modes (*cf.* McLaren 1991). A double-tilting goniometer stage capable of giving $\pm 30°$ of tilt above two orthogonal axes was used in all cases. Wherever possible, imaging was done under dynamical 2-beam diffraction conditions.

The TEM has been used to measure the CPO of quartz in the very fine grained bands, a technique used previously by Gapais & White (1982) and Mawer & Fitz Gerald (1993). Despite the drawback that only a small volume can be measured, a fuller description of the CPO can be obtained in contrast to the U-stage method, i.e. both the orientation of the *c*- and the *a*- axes can be determined. However, because no record was made of intensities of inequivalent reflections (e.g. *r* vs *z*), the diffraction symmetry of the quartz crystals was effectively treated as hexagonal (Mainprice *et al.* 1993, Mawer & Fitz Gerald 1993). While these are drawbacks when compared to SEM-based techniques such as channelling patterns and electron back-scatter diffraction (Schwarzer & Weiland 1988, Schwarzer 1990, Forwood & Clarebrough 1991, Lloyd *et al.* 1992, Mainprice *et al.* 1993, Randle 1992, 1993), these techniques provide only limited data on the intra- and intergrain defect structures. TEM can provide unique information on the

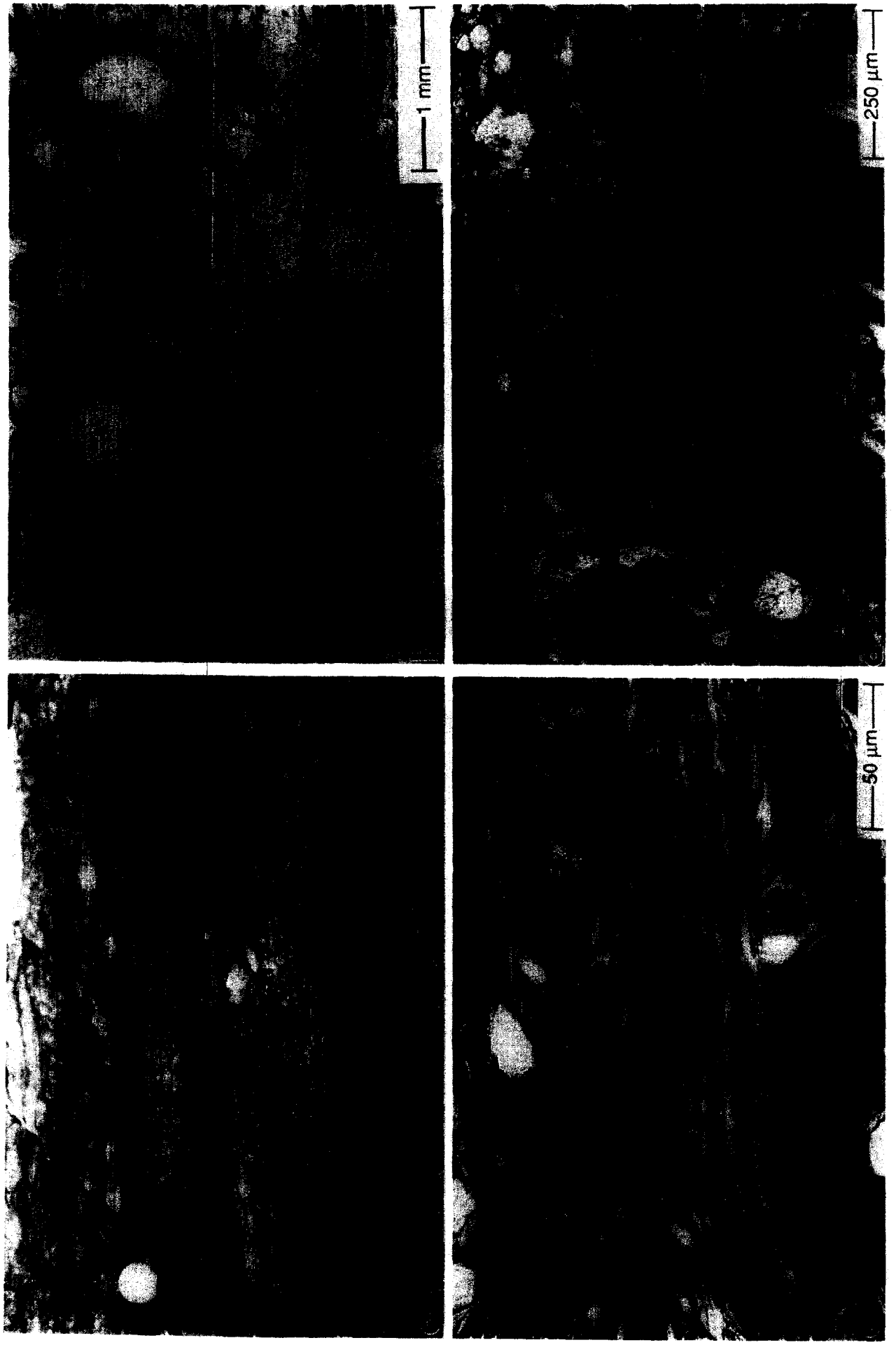

Fig. 2. (a) Field microstructure of a fine grained band (arrowed) within the quartzo-feldspathic mylonites of the RDZ at New Well; the coin is approximately 2 cm in diameter. Feldspar clasts characteristic of the mylonites are absent from the fine grained highly strained band. (b)–(d) Optical photomicrographs of a fine grained band (b and c) and of a hosting mylonite (d). (b) Large porphyroclasts of plagioclase, K-feldspar and epidote embedded in a matrix of finer grained bands of feldspar, plagioclase, quartz and biotite, ±epidote, alternating with quartz bands in a fine grained mylonite. (c) Quartz bands with domains of elongated quartzes with similar *c*-axis orientations parallel to the main foliation. (d) Low strain band; note that clast size and the grain size of quartzes are 10–20 times larger than in the high strain bands (e.g. b).

Fig. 3. Composite electron micrograph (bright field, BF) showing the microstructure of the quartz in a fine grained band. The larger grains are elongated parallel to the foliation and have well formed subgrains and high dislocation densities. The smaller grains consistently have a lower dislocation density and exhibit, if present, a disorganized cell structure. A line drawing of this area is given in Figs. 9 and 10.

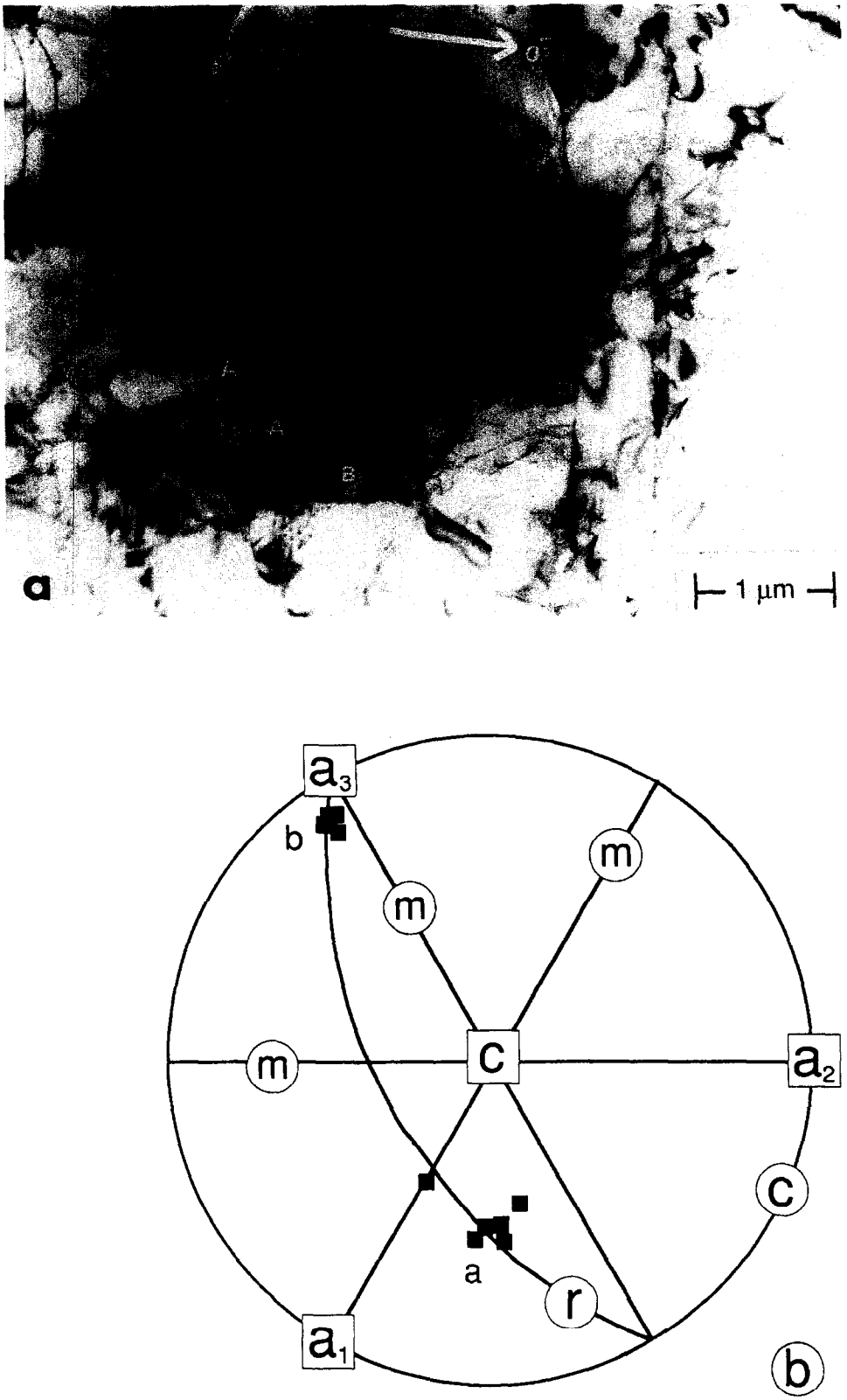

Fig. 4. (a) Composite electron micrograph (bright field, BF) showing dislocations within a larger grain. (b) Stereogram showing the orientation of the dislocation lines (labelled a & b in Fig. 4a) which lie on a rhombohedral plane (marked *r*).

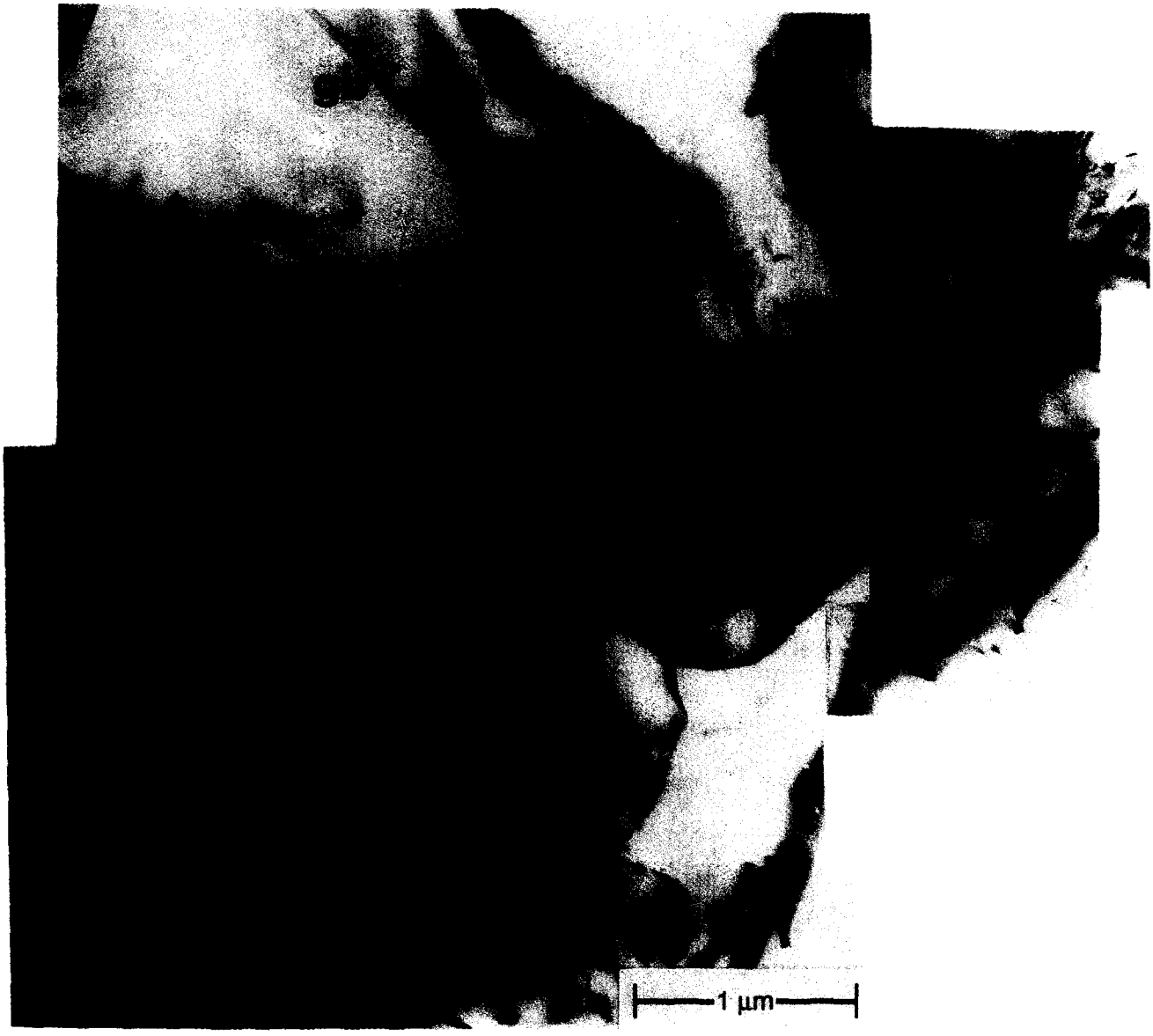

Fig. 5. Composite electron micrograph (bright field, BF) showing details of typical grain boundaries encountered. Both curved and straight grain boundaries occur. The curved boundaries (arrowed) bow towards regions of high defect densities; the region behind the curvature is virtually defect free. Note the lack of voids (bubbles) along the grain boundaries especially at triple points and at grain boundary–subgrain boundary intersections. **gb**: grain boundary; **sgb**: subgrain boundary.

correlation between the defect structure induced by deformation and the CPO.

The grain orientation measurement involved tilting the specimen so that a low index zone axis was parallel to the electron beam; the diffraction pattern and tilt angles were recorded [for more details on the technique the reader is referred to Edington (1974) and McLaren (1991)]. The diffraction patterns were obtained using 'microdiffraction' techniques outlined by McLaren (1991). The orientation of an individual grain is uniquely determined from the zone axes parallel to [*c*], ⟨*a*⟩, or normal to m, while for other cases at least two zone axes must be measured. Tilting errors were reduced by rotating into the low index zone from the same direction (i.e. always clockwise or counter-clockwise). The accuracy of the measurement is estimated at 2–3° (Schwarzer & Weiland 1988).

The grain and subgrain diameters were determined by taking the averages of the long and short axes directly from the micrographs and were subsequently corrected for sectioning effects using a factor 1.2 (*cf.* Underwood 1970). Measurements of numbers of free dislocations were carried out by counting dislocation terminations in a constant area ($\approx 0.5\,\mu m^2$) of the micrograph. Up to 100 subareas were counted in each foil studied, revealing large variations between the subareas. To avoid low counts, very thin areas in the foils were neglected. The free dislocation density is defined by the number per unit area of all linear lattice defects which appear not to be bound in subgrain walls or dislocation tangles.

As all of the grain size, subgrain size and dislocation density measurements generally reveal log-normal distributions (Ranalli 1984, Clark & Hosking 1986), the median (*Md*) of the distribution was taken as a measure of the grain size, subgrain size and dislocation density; half the interquartile range is taken as a measure of variability, whereas the skewness (*Sk*) and kurtosis (*Km*) are given to characterize the spread of data around the median.

Rapid irradiation damage prevented direct characterization of dislocation Burgers vectors (see Ardell *et al.* 1973, 1974). The $\mathbf{g}.\mathbf{b} = 0$ and the $\mathbf{g}.\mathbf{b} \times \mathbf{u} = 0$ criteria (*cf.* McLaren 1991) could not be used, as irradiated dislocations have a radial displacement or strain field, which has no unique relation to the original Burgers vector.

OPTICAL MICROSTRUCTURES AND TEXTURES

Detailed studies concentrated on the fine grained band shown in Fig. 2(a) with comparative studies in the surrounding coarser grained bands. The mylonite consists of porphyroclasts (up to 20% of the rock volume) of K-feldspar, plagioclase and epidote embedded in a very fine grained foliated matrix (Figs. 2b–d). The foliation is defined by the alignment of biotite flakelets. Inferred deformation conditions are at upper greenschist facies (*cf.* Obee & White 1985, Shaw & Black 1991). The porphyroclasts commonly have tails aligned parallel to the foliation.

Within both the fine and the coarse grained bands of the mylonite, most of the quartz occurs in discrete zones 10–200 μm thick (sub)parallel to the foliation (Figs. 2b–d), which alternate with continuous bands of finer grained K-feldspar, plagioclase, biotite, quartz ± epidote. Most of the K-feldspar and plagioclase clasts are embedded within such bands, suggesting that the latter originated from the porphyroclasts and have been simply rolled out by progressive deformation. This implies that the fine grained bands are the higher strained equivalents of the coarse grained bands and arose because of strain partitioning. So, the size and number of porphyroclasts decreases with increasing strain and the grain size of quartz reduces from 30–50 μm (Fig. 2d), to below 10 μm (see next section).

The grains within the quartz ribbons occur in domains oblique to the foliation with similar *c*-axis orientation. Within the fine grained bands these domains have a size between 10 and 30 μm (Fig. 2c) and show a very fine, patchy undulatory extinction. The individual domains are elongated and may be (sub)parallel (Fig. 2c) or oblique (up to 25°) to the main foliation. The quartz domains of the fine grained bands show a *c*-axis pattern similar to, but stronger than, that of the quartz grains from the coarse grained bands (Fig. 6). The *c*-axis textures are asymmetric type 1 girdles with respect to the foliation (Lister 1977), with a high density of *c*-axes in the centre of the pole figure. The sense of asymmetry is consistent with a reverse movement in the shear zone. The pole figures are similar to quartz *c*-axis textures previously measured in similar rock types along the Redbank Deformed Zone (Obee & White 1986).

ELECTRON MICROSCOPY

The deformation microstructures of quartz from the fine grained bands (*cf.* Figs. 2b & c) have been studied using TEM. At this scale (Fig. 3), the individual grains are elongate with a grain size ranging from 1 to 10 μm (*Md*: 2.3 ± 0.8 μm; *Sk*: 1.7; *Km*: 2.6). This grain size is much less than the thickness of an optical thin section and can account for the patchy undulatory extinction observed with the optical microscope. The free dislocations within the larger grains (typically >2.5 μm) are either curved or straight (Fig. 4) and tangles resulting from interacting dislocations are observed. These larger grains commonly have well formed slightly curved and straight low angle subgrain boundaries which are preferentially aligned either parallel or perpendicular to the direction of grain elongation (Fig. 3).

The free dislocation densities (*Md*: $6.5 \pm 2.8 \times 10^8$ cm^{-2}; *Sk*: 0.3; *Km*: −0.6) and subgrain sizes (*Md*: 2.1 ± 0.6 μm; *Sk*: 0.7; *Km*: −0.3) vary inhomogeneously throughout the sample (Fig. 7) with a general association of higher dislocation densities and larger subgrains with the larger grains and lower densities and smaller or no subgrains with the smaller grains (Fig. 7). Trace

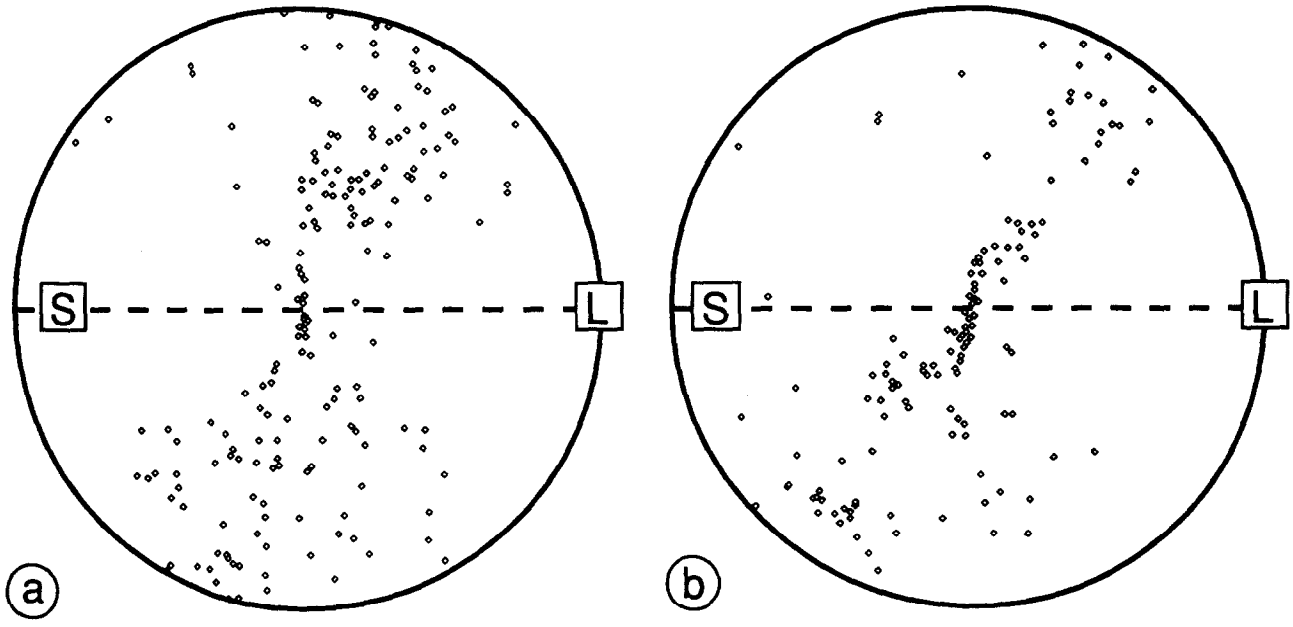

Fig. 6. Quartz *c*-axis fabrics, optical measurements. (a) Coarse grained bands (*cf.* Fig. 2d); $N = 190$. (b) Fine grained bands (*cf.* Fig. 2c); $N = 144$. The foliation (S) is vertical with the extension lineation (L) at the edge of the fabric diagram.

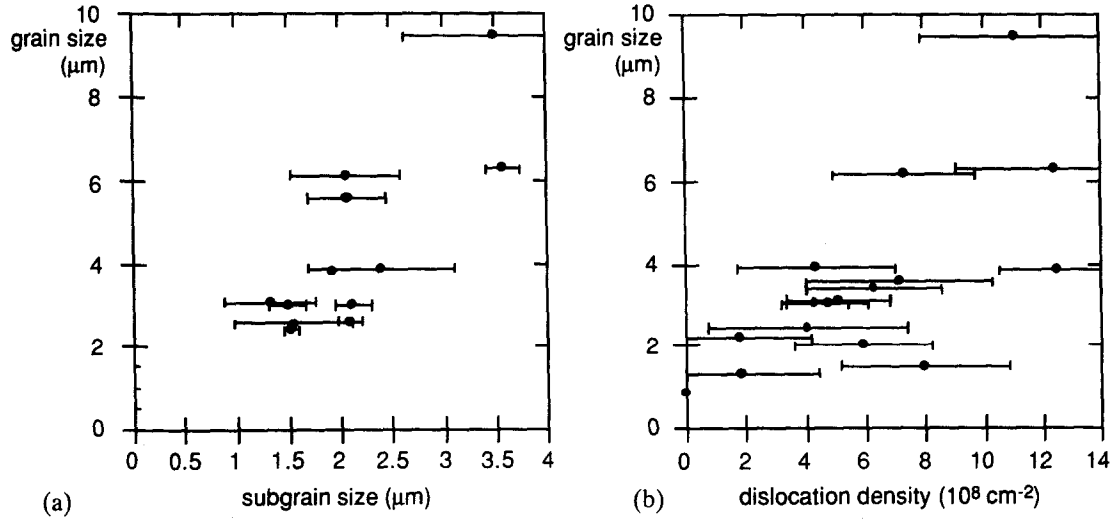

Fig. 7. Variations of subgrain size (a) and dislocation density (b) with grain size for the studied quartz band.

analyses of curved dislocations and dislocation loops were carried out and revealed that these dislocations commonly lie on rhombohedral crystallographic planes (Fig. 4) and, less commonly, on basal planes. The data presented in Fig. 4 are typical for all grains studied. Small bubbles are present on many dislocations and dislocation junctions.

Commonly, the high angle grain boundaries are approximately straight and (sub)parallel to the grain elongation. Small bubbles and voids do occur at the grain boundaries but are not common. Curved high angle grain boundaries are observed which bow towards a region of high defect density: i.e. a dislocation network or towards a tangle of dislocations (Fig. 5). The region behind the curvature commonly has a lower defect density. This observation suggests that grain boundary migration has occurred (*cf.* Beck & Sperry 1950; White 1976).

TEXTURE ANALYSES

Crystallographic Preferred Orientation (CPO)

The results of the CPO analyses of quartz from a fine grained band using TEM are shown in Fig. 8; three different areas were analysed. The grain elongation in the areas studied is subparallel to the foliation seen optically. Both the *c*- and *a*-axes reveal a strong preferred orientation. The *c*-axes lie on a great circle girdle asymmetrically arranged to the foliation; the *a*-axes occur in three distinct maxima, with one about 20° off the optically determined lineation. The fabric measured with the TEM is similar to the one obtained optically from the quartz domains from the fine grained bands (Fig. 6b). The main difference is the absence of *c*-axes lying at high angles to the foliation. This is probably due to preferred sampling, in TEM, of grains with a *c*-axis

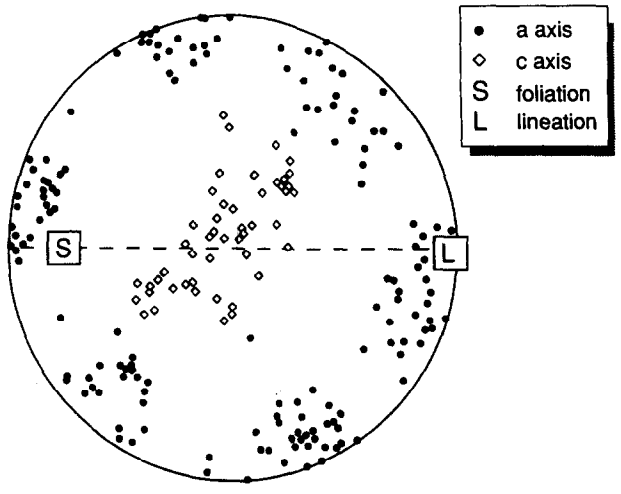

Fig. 8. Pole figure showing the crystallographic preferred orientation of *c*- and *a*-axes of quartz from a fine grained band measured using TEM. The foliation is marked *S* and the stretching lineation is marked *L*. $N = 50$.

perpendicular to the plane of the section, an orientation of high density measured optically (Fig. 6b).

The measured fabric shows many similarities with ones measured by Schmid & Casey (1986) in upper greenschist to lower amphibolite facies coarse grained tectonites (*cf.* their specimens CC1 and P248). The latter show a tendency for the high density area of *c*-axes to spread along a great circle girdle, somewhat inclined to the macroscopic fabric axes. A strong *a*-axes maximum at the margin of the pole figure is situated at an angle of less than 30° to the lineation. The microstructure (White *et al.* 1978) of CC1, a coarse grained (>>30 μm) mylonite, is characterized by nearly equant grains with well equilibrated grain boundaries and with dislocation substructures indicative of dislocation creep processes being important in the deformation (White *et al.* 1978).

Axes and angles of finite misorientation

When using the TEM to measure the CPO, information about all the crystallographic directions can be obtained. This allows the relationship between two adjacent grains or subgrains to be determined by means of an axis and angle of (finite) misorientation (Randle & Ralph 1986, Randle 1992). The axis of misorientation is a direction which is common to both the adjacent grains or subgrains and about which one must be rotated, by the angle of misorientation, in order to achieve the orientation of the other (Turner & Weiss 1963, Randle & Ralph 1986). This axis of misorientation becomes the axis of external rotation (*cf.* Turner & Weiss 1963, p. 328) if one of the crystals is fixed with respect to an external reference frame.

There are two basic approaches for the determination of axis/angle pairs from diffraction patterns. The first approach relies on standard crystallographic procedures and involves bisecting the angles between corresponding crystallographic planes of adjacent grains or subgrains (for details see Turner & Weiss 1963, p. 328, Randle & Ralph 1986). The second method, and the one used in this study, characterizes the misorientation by a 3×3 orthonormal matrix whose columns represent the direction cosines of the first grain referred to the second grain (for details see Randle 1992, 1993).

Quartz was treated as possessing hexagonal symmetry, and therefore there are 12 crystallographically equivalent ways of indexing each grain, and 144 ways of expressing the misorientation (Grimmer 1980). These misorientations occur in groups of 12, with members of each group having the same angle of misorientation and rotation axes which are symmetrically equivalent. Consequently, a misorientation between two hexagonal grains can be described in 12 different — but equivalent — ways, which in turn give 12 solutions of the axis/angle pair (Grimmer 1980, Forwood & Clarebrough 1991, Randle 1993). Any of these 12 misorientations may be chosen as they are physically indistinguishable. Commonly, the axis/angle pair giving the smallest possible rotation is chosen as the misorientation (see also Randle & Ralph 1986, Randle 1992, 1993, Mainprice *et al.* 1993) and this is the approach adopted in this study.

Because the accuracy in the CPO data is 2–3°, the measured axis/angle pair of misorientation may deviate from its true value. This error depends on the angle of misorientation between the two crystals: for large angles (>10°), error in both the axis and the angle is 5°, but for smaller angles (<10°) the error in the axis is increased to about 10–12°, while the error in the angle remains 5°.

A detailed analysis of the axes/angles of finite misorientation for a quartz ribbon area (*cf.* Fig. 3) is given in Figs. 9, 10 and 11. Figure 9(b) shows the angles of finite misorientation between adjacent grains and subgrains measured along three foil traverses as indicated in Fig. 9(a), one parallel (traverse I) and two perpendicular (traverses II and III) to the grain elongation. In the profiles, the angles of finite misorientation are presented with respect to the orientation of the first grain and are cumulative. Looking down the axis of finite misorientation, the angle of finite misorientation is taken negative for a counter clockwise and positive for a clockwise rotation. For example, in traverse II, at the boundary *k*, grain 7 has an angle of finite misorientation with grain 3 of +44°, across boundary *l* grain 8 makes an angle of +8° with grain 7 and 52° with grain 3. At boundary *p*, grain 4 has an angle of finite misorientation with grain 3 of +11°. The trajectories along which the *c*- and *a*-axes of the grains and subgrains rotate are shown on the stereographic plots in Fig. 9(b).

As can be seen in traverse II in Fig. 9(b), the misorientation between adjacent grains is very variable. The angle of finite misorientation changes in sign and magnitude across the profile, so that the cumulative angle shows a spiky pattern. Within one grain however, the finite misorientation shows a progressive increase (traverse I between boundaries *b* and *f*) or decrease (traverse III between boundaries *u* and *x*), with all of the walls having a similar sense of misorientation.

The axial distribution analysis (A.V.A.) of *c*-axis preferred orientation (Fig. 10) shows the presence of domains which are elongated parallel to the foliation

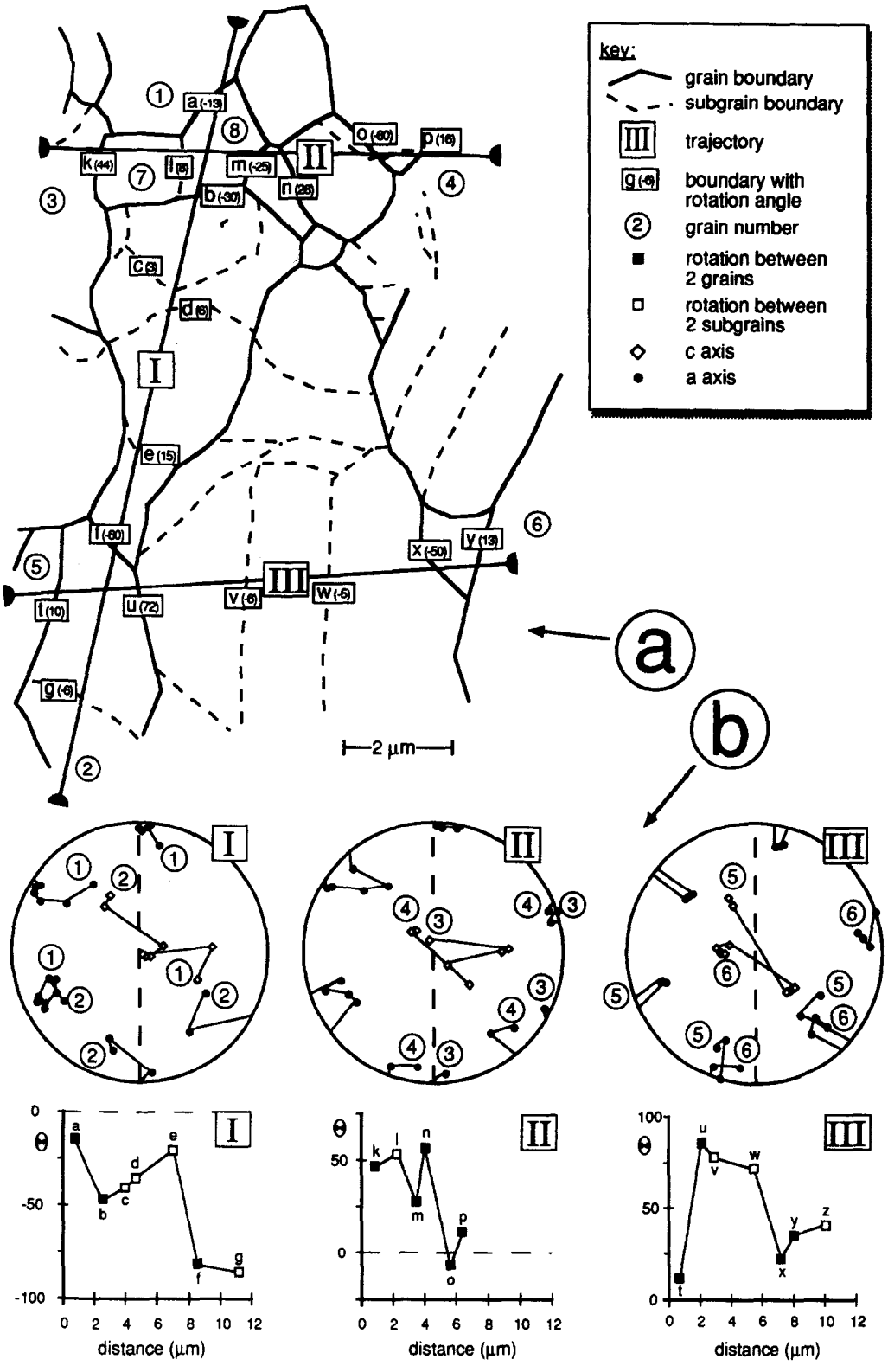

Fig. 9. Microtextural analyses of lattice misorientations across grain and subgrain boundaries of a quartz ribbon area. (a) Line drawing is after the composite electron micrograph given in Fig. 3. Three trajectories (I, II, III), along which the angles of misorientation have been measured, are indicated. Individual boundaries are marked a–y. The number accompanying each boundary is the angle of misorientation; positive angles are clockwise when looking down the axis of misorientation and negative if counterclockwise. (b) A stereographic plot of the *c*- and *a*-axes and a profile along each trajectory marked in Fig. 9(a). The numbers refer to grains shown in (a). The profiles present the angles of finite misorientation with respect to the orientation of the first grain (see text for discussion).

and are comparable in size and shape to the domains seen optically (Fig. 2c). The traces of the axes of finite misorientation between adjacent grains and subgrains are shown in this A.V.A. as arrows. The length of the arrow in Fig. 10(a) corresponds to the plunge of the axis in the stereographic plot (Fig. 11), i.e. the larger the arrow the smaller the plunge.

The axes of misorientation measured between grains

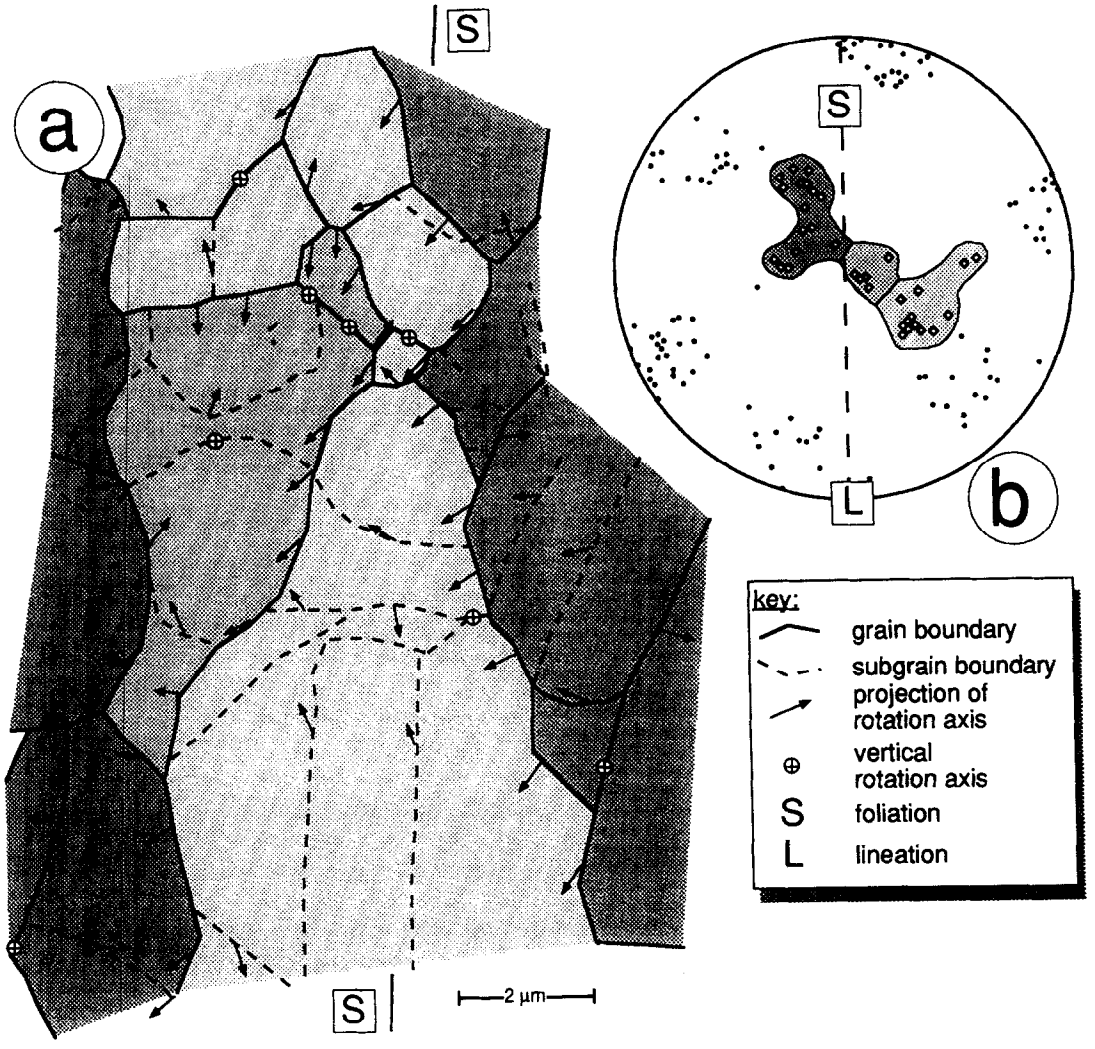

Fig. 10. (a) Axial distribution analysis (A.V.A.) diagram of the same area as Fig. 3 and Fig. 9. The shading of the different grains and subgrains reflects the grain's position in the CPO diagram given in (b). Traces of axes of finite misorientation between adjacent grains and subgrains are shown in the A.V.A. Note the domainal microstructure present in the studied area (see text for discussion).

and subgrains within the A.V.A. domains (Fig. 11a) show a preferred orientation within a great circle girdle lying (sub)parallel to the foliation plane with a high density area in the centre of the pole figure. As can be seen in Fig. 11(a) the axes between subgrains (open squares) are (sub)parallel to those between grains (filled squares). The axes measured between grains of different A.V.A. domains however (Fig. 11b), show a strong preferred orientation with a maximum lying at the edge of the pole figure inclined 45° to the foliation.

Slip systems

Due to rapid irradiation damage, the Burgers vectors of the dislocations could not be determined. However, if a crystal is divided into subgrains, the geometry of the subgrain boundary (dislocation lines, boundary orientation, axis/angle pair of misorientation) can be used to elucidate the active slip systems, by using Frank's formula (Amelinckx & Dekeyser 1959, Forwood & Clarebrough 1991). Frank's formula states that the axis of misorientation between two subgrains should be perpendicular to the net Burgers vector of the dislocations required to accommodate the misorientation at a subgrain boundary. Any low angle subgrain boundary can be formed with one, two or three dislocation families (Forwood & Clarebrough 1991). Dislocations with the same Burgers vector and the same line direction belong to the same dislocation family. If a subgrain wall is composed either of one or two dislocation families, or three dislocation families with coplanar Burgers vectors, the axis of misorientation will be perpendicular to all of the Burgers vectors of the dislocations within the subgrain boundary (Amelinckx & Dekeyser 1959, Trepied *et al.* 1980, Forwood & Clarebrough 1991). If the boundary is composed of three families of dislocations with non-coplanar Burgers vectors, then the axis of misorientation is not perpendicular to all of the Burgers vectors. Trepied *et al.* (1980) have shown that three non-coplanar Burgers vectors cannot produce a subgrain boundary in quartz.

With increasing dislocation content, the subgrain wall eventually becomes a high angle grain boundary. If there are no additional rotations arising from grain boundary sliding processes, the axis of misorientation will still be normal to the Burgers vectors in the (former

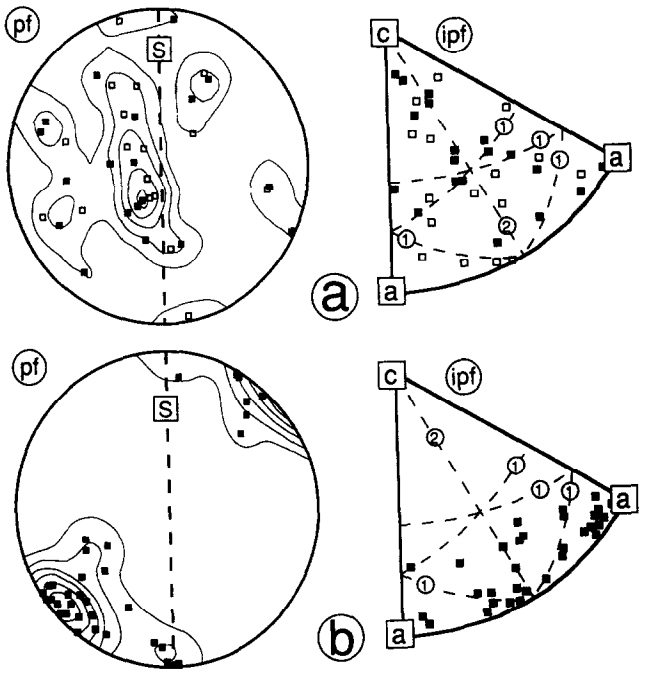

Fig. 11. Pole figures (pf) and inverse pole figures (ipf) of the axes of finite misorientation between adjacent grains and subgrains of the same area as Figs. 3, 9 and 10. (a) Axes of misorientation between grains (filled squares), where both belong to the same A.V.A. domain, are (sub)parallel to those between subgrains (open squares) and show a preferred orientation in the pf into a girdle parallel to the foliation. Contours are at 1, 2, 3 . . . times a uniform distribution. In the ipf, the axes show a tendency to lie on great circles perpendicular to $\langle c + a \rangle$ (marked 1) or $\langle a \rangle$ (marked 2). (b) The axes between grains from different A.V.A. domains show a strong maxima at the edge of the pole figure inclined at 45° to the foliation. Contours at 1, 3, 5 . . . times a uniform distribution. Most axes are either (sub)parallel to an *a*-axis or normal to an *m* plane (see text for discussion).

sub)grain boundary. For example, if a crystal is misoriented due to $\langle a \rangle$ edge dislocations, the axis of finite misorientation will lie in a plane normal to $\langle a \rangle$, which is an m plane. To find the Burgers vectors causing the misorientation between two subgrains or two grains involves calculating the angle between the axis of misorientation and any of the known Burgers vectors for quartz, i.e. [*c*], $\langle a \rangle$ and $\langle c + a \rangle$ (*cf.* Morrison-Smith *et al.* 1976). This analysis assumes that any purely geometrically necessary dislocations (White 1977) that accommodate the rotations within the subgrain walls are slip dislocations. Frank's formula was successfully applied, in a rigorous form, to slip plane analysis in quartz by Lloyd & Freeman (1991, 1994).

Frank's formula has been applied to the quartz ribbon area presented in Figs. 3 and 10 and described in the previous sections; the results are shown graphically in inverse pole figures (Fig. 11). The axes of misorientation between grains (filled squares) and subgrains (open squares) within the same A.V.A. domain (Fig. 11a) both show a tendency to lie on great circles perpendicular to either $\langle c + a \rangle$ (marked 1 in Fig. 11a) or $\langle a \rangle$ (marked 2 in Fig. 11a). This suggests that dislocations with $\langle c + a \rangle$ and $\langle a \rangle$ Burgers vectors have been operative in accommodating the misorientation between both subgrains and grains within the same A.V.A. domain.

Most of the rotation axes measured between grains of different A.V.A. domains are either (sub)parallel to an *a*-axis or normal to an *m* plane. Some spread of the axes exists in great circles perpendicular to $\langle c + a \rangle$ (marked 1 in Fig. 11b) and in a great circle perpendicular to $\langle a \rangle$ (marked 2 in Fig. 11b). These misorientation relations between grains of different A.V.A. domains were tested against the coincidence site lattice (CSL) theory (see Bollman 1970, Chapter 12) for hexagonal crystals (Bleris *et al.* 1982, McLaren 1986, Grimmer 1989a,b). The volume ratio of primitive cells for the CSL and crystal lattice is a positive integer Σ, called the multiplicity of the CSL (Grimmer 1989b). The smaller the value of Σ, the larger the coincidence and the better the 'fit' between the grains. In cubic crystals only boundaries with a $\Sigma < 49$ are considered to have a CSL (*cf.* Randle 1993). Brandon's criterion (*cf.* Randle 1993) has been used to calculate the maximum deviation from a CSL orientation. When the misorientation data presented in Fig. 11 are compared with the CSL relations calculated for quartz (McLaren 1986, his table 3) it is found that about 80% of the misorientation relations can be described as having a CSL with a Σ value lower than 49. Of these, 30% have $\Sigma = 16$ (30° rotation around an *a*-axis), 20% have $\Sigma = 6$ (48.9° rotation around normal to an m plane) and 10% have $\Sigma = 19$ (55.4° rotation around an *a*-axis).

DISCUSSION

The microstructural and microtextural observations indicate that flow in the fine grained quartz bands of the mylonite studied was due to dislocation creep processes, although the grain size is well below 10 μm (2.3 ± 0.8 μm). The pertinent observations are the presence of dislocations, subgrains and the sharp *c*- and *a*-axes CPO's. The analyses of the axis/angle of finite misorientation between grains indicate that there are no apparent additional rotations, other than those arising from dislocation creep processes. Additional rotations would be expected if grain boundary sliding had contributed significantly to the deformation (Beeré 1978). This view is supported by the results of Lartigue, Korinek & Dupau (1994) who measured, using TEM, the axes of finite misorientation between grains in fine grained, superplastically deformed, Mg-doped alumina in which grain boundary sliding had played a prominent role during deformation. They found additional rotations and using their data (their tables 1 and 2) it is possible to determine that the axes of rotation between grains are not perpendicular to any of the Burgers vectors known for alumina.

The misorientation relations between grains of different A.V.A. domains can be described as CSL relations which are associated with low energy grain boundary structures (*cf.* Gleiter 1982). It has been shown that CSL relations between grains can have a profound effect on the mechanical and chemical properties of grain boundaries, such as grain boundary migration, grain boundary diffusion, phase transformations and grain growth (*cf.* Gleiter 1982, Forwood & Clarebrough 1991, Peterson

1979, Smith *et al.* 1979, Bishop *et al.* 1979, Randle 1993). Haruna *et al.* (1992) showed that grain boundary sliding is also greatly affected by the presence of CSL boundaries. They compared measured offsets across lead grain boundaries in a superplastically deformed lead–tin alloy with the value of Σ. They observed that grain boundary sliding was difficult at lead grain boundaries with low Σ values, while rather easy at random boundaries with larger Σ values (>49). It is therefore unlikely that grain boundary sliding has occurred in the very fine grained quartz bands studied here, as 80% of the misorientation relations can be described as having a CSL with a Σ value lower than 49. This fact, plus the rotation data and the presence of characteristic dislocation structures, leads us to conclude that the dominant deformation mechanism within the fine grained quartz bands was by dislocation creep processes without significant grain boundary sliding. This conclusion is in contrast to that drawn in both the materials science literature (e.g. Padmanabhan & Davies 1980, Gifkins 1982, Langdon 1982, 1990) and the geological literature (e.g. Boullier & Gueguen 1975, White 1977, Gapais & White 1982, Behrmann 1985), which is, that with grain sizes below 10 μm, the deformation mechanism has a major component of grain boundary sliding with the materials having weak CPO's.

There is a strong slip component to the dislocation creep involving $\langle c + a \rangle$ slip together with $\langle a \rangle$. The role of $\langle c + a \rangle$ slip has always been controversial. Although dislocations with a $\langle c + a \rangle$ Burgers vector have only rarely been directly confirmed in naturally deformed quartz, they are known to occur experimentally (Baëta & Ashbee 1969a,b, Trepied & Doukhan 1982) in synthetic single crystals of quartz deformed at high temperatures and at differential stresses exceeding 200 MPa. We therefore suggest that $\langle c + a \rangle$ slip may take place in high stress environments in nature. Consequently we used microstructural features to get an indication whether the stresses during deformation were abnormally high. There are a number of methods available to determine the paleostress in mylonites deforming by dislocation creep (*cf.* Kohlstedt & Weathers 1980). It has long been known that the size of subgrains and recrystallized grains, and the free dislocation density are related to the magnitude of the differential stress responsible for the deformation of the polycrystal (Twiss 1977, Kohlstedt & Weathers 1980). Dislocation density is highly susceptable to changes in temperature and stress and commonly reflects a later stage stress-free anneal or a late stress pulse (White 1979a). The subgrain size and the recrystallized grain size are better indicators of the paleostress (White 1979a). For grain size, we must also consider the recrystallization mechanism (Twiss 1977, Drury *et al.* 1985). The paleopiezometric relations from Mercier *et al.* (1977) for the recrystallized grain size for quartz with the same recrystallization mechanism as observed in our study, *viz.* a rotation recrystallization mechanism, and from White (1979b) (using the experiments of Ardell *et al.* 1973) for subgrain size have been used to estimate the stress. The stresses estimated from the grain size (2.3 $\pm$ 0.8 μm) and subgrain size (2.1 $\pm$ 0.6 μm) are equal, with 220 $\pm$ 40 MPa and 250 $\pm$ 65 MPa, respectively. That is, the stresses appear to have been of sufficient magnitude to activate $\langle c + a \rangle$ slip.

The question arises as to the softening mechanism that allowed strain partitioning into the very fine grained bands. The usually invoked mechanism of a change to a grain size sensitive grain boundary mechanism is not appropriate in this instance (see above). The fine grain size appears to have been maintained by continual recrystallization. The evidence for this comes firstly from the tendency for the larger grains to have higher dislocation densities and well formed subgrains (Fig. 7), and secondly, from observations indicative of grain boundary migration (Fig. 5). We take these two pieces of evidence to indicate that grain growth occurred via grain boundary migration. As growth continues, the density of the internal dislocations increases and subgrains develop. This increase in internal strain energy and the increasing misorientation of subgrains leads to the preferential recrystallization of the large grains to maintain a quasi steady state grain size. The softening leading to strain partitioning in the very fine grained bands is believed to result from two factors. The first is the continual supply of grains free from dislocations or with low densities of dislocations. The second is due to geometrical softening, because the grains have their lattices reoriented so that their slip planes lie in or near the plane of shear and their slip directions come to lie parallel to the direction of shear (Bouchez 1978, Williams & Dixon 1982, Knipe & Law 1987). The CPO data (Fig. 8) indicate that mainly the rhombohedral and prism planes are (sub)parallel to the foliation plane with an *a*-axes maxima close to the lineation. Trace analysis (Fig. 4) revealed dominant rhombohedral slip planes, whereas the rotation axes indicated a major contribution of dislocations with $\langle c + a \rangle$ and $\langle a \rangle$ Burgers vector to the slip. A strong maximum of $\langle a \rangle$ axes is present near the stretching lineation (Fig. 8). Two sets of $\langle c + a \rangle$ dislocations on opposite sides of the lineation will result in slip towards the stretching lineation. It is therefore suggested that geometrical softening occurred due to this preferential alignment of rhombohedral planes parallel to the foliation.

The recrystallization mechanism that supplied the new mechanically soft grains and maintained the quasi steady state grain size involved the formation of high angle grain boundaries from low angle subgrain boundaries by a progressive misorientation across subgrain walls (*cf.* Urai *et al.* 1986, Drury & Urai 1990). The coarse grained quartz bands in the lower strain mylonites have *c*-axis patterns similar to the very fine grained quartz bands from the high strain mylonite studied (Figs 6a & b). The only difference is that the texture is sharper for the latter. The domainal microstructure of the very fine grained quartz ribbons therefore suggests a strong host grain control on the orientation of the newly formed grains. While microstructures indicative of local grain boundary migration have been observed, we have found no evidence for the formation of new strain free nuclei. Similar recrystallization mechanisms in quartz have

been reported by White (1973, 1977), Lloyd & Freeman (1991, 1994) and Knipe & Law (1987).

CONCLUSIONS

(1) Transmission electron microscopy investigations of the microstructure and microtexture of very fine grained quartz bands (2.3 ± 0.8 μm) in mylonites from the Redbank Deformed Zone of Central Australia, suggest that dislocation creep processes were the dominant deformation mechanism operative with $\langle c + a \rangle$ and $\langle a \rangle$ slip being important.

(2) Analyses of the axes and angles of finite misorientation between adjacent grains and subgrains indicate that there are no rotations of the type to be expected if grain boundary sliding had contributed significantly to the deformation.

(3) Softening and the maintenance of a quasi steady state grain size in the fine grained quartz bands was by continual recrystallization. The recrystallization mechanism included local grain boundary migration and the development of high angle grain boundaries from low angle subgrain boundaries by a progressive misorientation across subgrain walls, and resulted in host grain control of the orientation of the recrystallized grains.

(4) Stresses operative during the flow of the fine grained mylonite studied have been estimated to be in the range 220–250 MPa, which is high. They are however of the magnitude that may be required for the operation of $\langle c + a \rangle$ slip.

Acknowledgements—We would like to thank M. R. Drury, D van der Wal, H. L. M. van Roermund for their help, critical review and fruitful discussions. The Journal referees, G. E. Lloyd and J. D. Fitz Gerald, are thanked for their detailed comments on the manuscript. Timon Fliervoet wishes to thank J. Pieters, P. van Maurik, H. L. M. van Roermund, B. K. Smith and M. R. Drury for their help with and introduction to electron microscopy. A. Rekko, R. Shaw, B. Collins, D. Young and the people from the NTGS are kindly thanked for their help and logistical support during field work. This work is funded by the Netherlands Organisation of Scientific Research (NWO).

REFERENCES

Amelinckx, S. & Dekeyser, W. 1959. The structure and properties of grain boundaries. *Solid State Phys.* **8**, 325–499.

Ardell, A. J., Christie, J. M. & McCormick, J. W. 1974. Dislocation images in quartz and the determination of Burgers vectors. *Phil. Mag.* **29**, 1399–1411.

Ardell, A. J., Christie, J. M. & Tullis, J. 1973. Dislocation substructures in deformed quartz rocks. *Crystal Lattice Defects* **4**, 275–285.

Baëta, R. D. & Ashbee, K. H. G. 1969a. Slip systems in quartz: I. experiments. *Am. Miner.* **54**, 1551–1573.

Baëta, R. D. & Ashbee, K. H. G. 1969b. Slip systems in quartz: II. Interpretation. *Am. Miner.* **54**, 1574–1582.

Beck, P. A. & Sperry, P. R. 1950. Strain induced grain boundary migration in high purity aluminium. *J. appl. Phys.* **21**, 150.

Beeré, W. 1978. Stresses and deformation at grain boundaries. *Phil. Trans. R. Soc. Lond.* **A 288**, 177–196.

Behrmann, J. H. 1985. Crystal plasticity and superplasticity in quartzite: a natural example. *Tectonophysics* **115**, 101–129.

Behrmann, J. H. & Mainprice, D. 1987. Deformation mechanisms in a high-temperature quartz-feldspar mylonite: evidence for superplastic flow in the lower continental crust. *Tectonophysics* **140**, 297–305.

Berthé, D., Choukroune, P. & Jegouzo, P. 1979. Orthogneiss, mylonite and non-coaxial deformation of granites: the example of the South Armorican Shear zone. *J. Struct. Geol.* **1**, 31–42.

Bishop, G. H., Harrison, R. J., Kwok, T. & Yip, S. 1979. Comments on sliding and migration based on computer molecular dynamics simulations of grain boundaries. In: *Grain Boundary Structure and Kinetics* (edited by Balluffi, R. W.). ASM, Metals Park, 373–377.

Bleris, G. L., Nouet, G., Hagège & Delavignette, P. 1982. Characterization of grain boundaries in the hexagonal system based on tables of coincidence site lattices (CSL's). *Acta Cryst.* **A38**, 550–557.

Bollmann, W. 1970. *Crystal Defects and Crystalline Interfaces*, Springer-Verlag, Berlin.

Bossière, G. & Vauchez, A. 1978. Déformation naturelle par cisaillement ductile d'un granite de Grande Kabylie occidentale (Algérie). *Tectonophysics* **51**, 57–81.

Bouchez, J. L. 1978. Preferred orientations of quartz $\langle a \rangle$ axes in some tectonites: kinematic inferences. *Tectonophysics* **49**, T25–T30.

Boullier, A. M. & Gueguen, Y. 1975. Origin of some mylonites by superplastic flow. *Contrib. Mineral Petrol.* **50**, 93–104.

Carter, N. L. & Tsenn, M. C. 1987. Flow properties of continental lithosphere. *Tectonophysics* **136**, 27–63.

Choukroune, P. & ECORS-team 1989. The ECORS Pyrenean deep seismic profile: reflection data and the overall structure of an orogenic belt. *Tectonics* **8**, 23–39.

Clark, W. A. V. & Hosking, P. L. 1986. *Statistical Methods for Geographers*. John Wiley and Sons, New York.

Drury, M. R. & Humphreys, F. J. 1988. Microstructural shear criteria associated with grain-boundary sliding during ductile deformation. *J. Struct. Geol.* **10**, 83–89.

Drury, M. R., Humphreys, F. J. & White, S. H. 1985. Large strain deformation studies using polycrystalline magnesium as a rock analogue. Part II: dynamic recrystallisation mechanisms at high temperatures. *Phys. Earth & Planet. Sci.* **40**, 208–222.

Drury, M. R. & Urai, J. L. 1990. Deformation-related recrystallization processes. *Tectonophysics* **172**, 235–253.

Edington, J. W. 1974. *Monographs in Practical Electron Microscopy in Materials Science*, Philips Technical Library, The Macmillan Press Ltd, London.

Etheridge, M. A. & Wilkie, J. C. 1979. Grainsize reduction, grain boundary sliding and the flow strength of mylonites. *Tectonophysics* **58**, 159–178.

Evans, B., Rowen, M. & Brace, W. F. 1980. Grain-size sensitive deformation of stretched conglomerate from Plymouth, Vermount. *J. Struct. Geol.* **2**: 411–424.

Forwood, C. T. & Clarebrough, L. M. 1991. *Electron Microscopy of Interfaces in Metals and Alloys*. IOP Publishing, Bristol.

Gapais, D. & White, S. H. 1982. Ductile shear bands in a naturally deformed quartzite. *Textures and Microstructures* **5**, 1–17.

Gifkins, R. C. 1982. Mechanisms of superplasticity. In: *Superplastic Forming of Structural Alloys* (edited by Baton, N. E. & Hamilton, C. H.). AIME, Warrendale, 3–26.

Gleiter, H. 1982. On the structure of grain boundaries in metals. *Mat. Sci. Eng.* **52**, 91–131.

Goleby, B. R., Shaw, R. D., Wright, C., Kennet, B. L. N. & Lambeck, K. 1989. Geophysical evidence for 'thick-skinned' crustal deformation in central Australia. *Nature* **337**, 325–330.

Grimmer, H. 1980. A unique description of the relative orientation of neighbouring grains. *Acta Cryst.* **A36**, 382–389.

Grimmer, H. 1989a. Systematic determination of coincidence orientations for all hexagonal lattices with axial ratio c/a in a given interval. *Acta Cryst.* **A45**, 320–325.

Grimmer, H. 1989b. *Coincidence Orientations of Grains in Rhombohedral and Hexagonal Materials*. Paul Scherrer Institut, Würlingen.

Haruna, T., Shibayanagi, T., Hori, S. & Furushiro, N. 1992. Effect of grain boundary characters on grain boundary sliding during superplastic deformation. *Trans Materials JIM.* **33**, 374–379.

Hirth, G. & Tullis, J. 1992. Dislocation creep regimes in quartz aggregates. *J. Struct. Geol.* **14**, 145–159.

Jaoul, O., Tullis, J. & Kronenberg, A. 1984. The effect of varying water contents on the creep behavior of Heavitree quartzite. *J. geophys. Res.* **89**, 4298–4312.

Knipe, R. J. & Law, R. D. 1987. The influence of crystallographic orientation and grain boundary migration on microstructural and textural evolution in an *S–C* mylonite. *Tectonophysics* **135**, 155–169.

Kohlstedt, D. L. & Weathers, M. S. 1980. Deformation-induced microstructures, paleopiezometers, and differential stresses in deeply eroded fault zones. *J. geophys. Res.* **85**, 6269–6285.

Langdon, T. G. 1982. Experimental observations in superplasticity. In: *Superplastic Forming of Structural Alloys* (edited by Paton, N. E. & Hamilton, C. H.). AIME, Warendale, 27–40.

Langdon, T. G. 1990. Superplastic ceramics. They're not a stretch of the imagination anymore. *JOM*. 8–13.

Lartigue Korinek, S. & Dupau, F. 1994. Grain boundary behavior in superplastic Mg-doped alumina with Yttria codoping. *Acta Metall. Mater.* **42**, 293–302.

Law, R. D., Knipe, R. J. & Dayan, H. 1984. Strain path partitioning within thrust sheets: microstructural and petrofabric evidence from the Moine Thrust zone at Loch Eriboll, northwest Scotland. *J. Struct. Geol.* **6**, 477–497.

Lister, G. L. 1977. Crossed-girdle *c*-axis fabrics in quartzites plastically deformed by plane strain and progressive simple shear. *Tectonophysics* **39**, 51–54.

Lloyd, G. E. & Freeman, B. 1991. Dynamic recrystallization of a quartz porphyroclast. *Textures and Microstructures* **14–18**, 751–756.

Lloyd, G. E. & Freeman, B. 1994. Dynamic recrystallization under greenschist facies conditions. *J. Struct. Geol.* **16**, 867–881.

Lloyd, G. E., Law, R. D., Mainprice, D. & Wheeler, J. 1992. Microstructural and crystal fabric evolution during shear zone formation. *J. Struct. Geol.* **14**, 1079–1100.

Mainprice, D., Lloyd, G. E. & Casey, M. 1993. Individual orientation measurements in quartz polycrystals: advantages and limitations for texture and petrophysical property determinations. *J. Struct. Geol.* **15**, 1169–1187.

Mawer, C. K. & Fitzgerald, J. D. 1993. Microstructure of kink band boundaries in naturally deformed Chewings Range quartzite. In: *Defects and Processes in the Solid State: Geoscience Applications. The McLaren Volume* (edited by Boland, J. N. & Fitz Gerald, J. D.). *Developments in Petrology* **14**, 49–67. Elsevier, Amsterdam.

McGeary, S. & Warner, M. R. 1985. Seismic profiling the continental lithosphere. *Nature* **317**, 795–797.

McLaren, A. C. 1986. Some speculations on the nature of high-angle grain boundaries in quartz rocks. In: *Mineral and Rock Deformation: Laboratory Studies, The Paterson Volume* (edited by Hobbs, B. E. & Heard, H. C.). *Geophys. Monogr. Ser.* **36**, 233–245. AGU, Washington D.C.

McLaren, A. C. 1991. *Transmission Electron Microscopy of Minerals and Rocks*. Cambridge University Press, Cambridge.

Mercier, J. C., Anderson, D. A. & Carter, N. L. 1977. Stress in the lithosphere: inferences from steady state flow of rocks. *Pure & Appl. Geophys.* **115**, 199–226.

Mitra, S. 1976. A quantitative study of deformation mechanisms and finite strain in quartzites. *Contrib. Mineral. Petrol.* **59**, 203–226.

Morrison-Smith, D. J., Patterson, M. S. & Hobbs, B. E. 1976. An electron microscope study of plastic deformation in single crystals of synthetic quartz. *Tectonophysics* **33**, 43–79.

Obee, H. K. & White, S. H. 1985. Faults and associated fault rocks of the Southern Arunta block, Alice Springs, Central Australia. *J. Struct. Geol.* **7**, 701–712.

Obee, H. K. & White, S. H. 1986. Microstructural and fabric heterogeneities in fault rocks associated with a fundamental fault. *Proc. R. Soc. Lond* **A317**, 99–109.

Ord, A. & Hobbs, B. E. 1989. The strength of the continental crust, detachment zones and the development of plastic instabilities. *Tectonophysics* **158**, 269–289.

Padmanabhan, K. A. & Davies, G. J. 1980. *Superplasticity*. Springer-Verlag, Berlin.

Peterson, N. L. 1979. Grain-boundary diffusion—structural effects, models, and mechanisms. In: *Grain Boundary Structure and Kinetics* (edited by Balluffi, R. W.). ASM, Metals Park, 209–238.

Ranalli, G. 1984. Grain size distribution and flow stress in tectonites. *J. Struct. Geol.* **6**, 443–447.

Randle, V. 1992. *Microtexture Determination and its Applications*. Institute of Materials, London.

Randle, V. 1993. *The Measurement of Grain Boundary Geometry*. IOP Publishing, Bristol.

Randle, V. & Ralph, B. 1986. A practical approach to the determination of the crystallography of grain boundaries. *J. Mat. Sci.* **21**, 3823–3828.

Rutter, E. H., Casey, M. & Burlini, L. 1994. Preferred crystallographic orientation development during the plastic and superplastic flow of calcite rocks. *J. Struct. Geol.* **16**, 1431–1446.

Schmid, S. M. & Casey, M. 1986. Complete fabric analysis of some commonly observed quartz *c*-axis patterns. In: *Mineral and Rock Deformation: Laboratory Studies, The Paterson Volume* (edited by Hobbs, B. E. & Heard, H. C.). *Geophys. Monogr. Ser.* **36**, 263–296. AGU, Washington D.C.

Schwarzer, R. A. 1990. Measurement of local textures with transmission electron and scanning electron microscopes. *Textures and Microstructures* **13**, 15–30.

Schwarzer, R. A. & Weiland, H. 1988. Texture analysis by the measurement of individual grain orientations—Electron microscopical methods and application on dual phase steel. *Textures and Microstructures* **8–9**, 551–577.

Shaw, R. D. & Black, L. P. 1991. The history and tectonic implications of the Redbank Thrust Zone, central Australia, based on structural, metamorphic and Rb–Sr isotopic evidence. *Aust. J. Earth Sci.* **38**, 307–332.

Simpson, C. 1985. Deformation of granitic rocks across the brittle–ductile transition. *J. Struct. Geol.* **7**, 503–511.

Smith, D. A., Rae, C. M. F. & Grovenor, C. R. M. 1979. Grain boundary migration. In: *Grain Boundary Structure and Kinetics* (edited by Balluffi, R. W.). ASM, Metals Park, 337–371.

Stünitz, H. & Fitz Gerald, J. D. 1993. Deformation of granitoids at low metamorphic grade. II: Granular flow in albite-rich mylonites. *Tectonophysics* **221**, 299–324.

Trepied, L. & Doukhan, J. C. 1982. Evidence of <*a*+*c*> dislocations in synthetic quartz single crystals compressed along the *c* axis. *Bull. Mineral.* **105**, 176–180.

Trepied, L., Doukhan, J. C. & Paquet, J. 1980. Subgrain boundaries in quartz. Theoretical analysis and microscopic observations. *Phys. Chem. Minerals.* **5**, 201–218.

Tullis, J., Christie, J. M. & Griggs, D. T. 1973. Microstructures and preferred orientations of experimentally deformed quartzites. *Bull. Geol. Soc. Am.* **84**, 297–314.

Turner, F. J. & Weiss, V. 1963. *Structural Analysis of Metamorphic Tectonites*. McGraw-Hill, New York.

Twiss, R. J. 1977. Theory and applicability of a recrystallized grain size paleopiezometer. *Pure & Appl. Geophys.* **115**, 227–244.

Underwood, E. E. 1970. *Quantitative Stereology*. Addison-Wesley Publishing Company, Reading, Massachusetts.

Urai, J. L., Means, W. D. & Lister, G. S. 1986. Dynamic recrystallization of minerals. In: *Mineral and Rock Deformation: Laboratory Studies, The Paterson Volume* (edited by Hobbs, B. E. & Heard, H. C.). *Geophys. Monogr. Ser.* **36**, 161–199. AGU, Washington D.C.

Vernon, R. H. & Flood, R. H. 1988. Contrasting deformation and metamorphism of S- and I-type granitoids in the Lachlan Fold Belt, eastern Australia. *Tectonophysics*, **147**, 127–143.

Watts, M. J. & Williams, G. D. 1979. Fault rocks as indicators of progressive shear deformation in the Guingamp region of Brittany. *J. Struct. Geol.* **1**, 323–332.

White, S. H. 1973. Syntectonic recrystallization and texture development in quartz. *Nature* **244**, 267–268.

White, S. H. 1976. The effects of strain on the microstructures, fabrics, and deformation mechanisms in quartzites. *Phil. Trans. R. Soc. Lond.* **A283**, 69–86.

White, S. H. 1977. Geological significance of recovery and recrystallization processes in quartz. *Tectonophysics* **39**, 143–170.

White, S. H. 1979a. Difficulties associated with paleostress estimates. *Bull. Mineral.* **102**, 210–215.

White, S. H. 1979b. Grain and sub-grain size variations across a mylonite zone. *Contrib. Mineral. Petrol.* **70**, 193–202.

White, S. H. 1979c. Paleostress estimates in the Moine thrust, Eriboll, Scotland. *J. Struct. Geol.* **280**, 222–223.

White, S. H., Bretan, P. G. & Rutter, E. H. 1986. Fault-zone reactivation: kinematics and mechanisms. *Phil. Trans. R. Soc. Lond.* **A317**, 81–97.

White, S. H., Burrows, S. E. & Carreras, J. 1978. Textural and microstructural development in a naturally deformed quartzite: a metallurgical approach. In: 5th Int. Conf. on Textures of Materials (edited by Gottstein, G. & Luecke, K.). Aachen, Germany **2**, 211–220.

White, S. H., Burrows, S. E., Carreras, J., Shaw, N. D. & Humphreys, F. J. 1980. On mylonites in ductile shear zones. *J. Struct. Geol.* **2**, 175–187.

Williams, G. & Dixon, J. 1982. Reaction and geometrical softening in granitoid mylonites. *Textures and Microstructures* **4**, 223–239.